applied sciences

MDPI

Article

Comprehensive Modeling of CO_2 Sequestration in Syderiai Deep Saline Aquifer: Insights into Leakage, Geo-Mechanical Changes, and Geo-Chemical Impacts

Shankar Lal Dangi [1], Shruti Malik [1], Ravi Sharma [2] and Mayur Pal [1,*]

[1] Department of Mathematical Modeling, Kaunas University of Technology, LT-51368 Kaunas, Lithuania; shankar.dangi@ktu.edu (S.L.D.); shruti.malik@ktu.lt (S.M.)
[2] Department of Earth Sciences, Indian Institute of Technology, Roorkee 247667, India; ravi.sharma@es.iitr.ac.in
* Correspondence: mayur.pal@ktu.lt

Abstract

This paper presents a comprehensive study on the feasibility and implications of a CO_2 injection simulation in the Syderiai deep saline aquifer of Lithuania, focusing on leakage, geo-mechanical aspects, and geo-chemical aspects. The Syderiai aquifer, characterized by its sandstone formation covered by shaly rocks, is considered a potential site for CO_2 geological storage in Lithuania. Using 3D mechanistic models developed in T-navigator software, we conducted extensive simulations to analyze CO_2 storage behavior and associated impacts. The leakage study examines various scenarios to assess the impact of fracture permeability, layer-wise heterogeneity, and fracture position on CO_2 injection and leakage volumes. Results indicate that while fracture permeability influences CO_2 migration dynamics, its impact on both free and dissolved CO_2 leakage volumes is minimal, highlighting that leakage behavior is more dependent on the presence of fractures than their permeability. Geo-mechanical analysis reveals the effects of CO_2 injection on the bulk modulus and shear modulus of sandstone and shale formations, highlighting changes in compaction and cementation. The geo-chemical study was performed using TOUGHREACT software V4.13-OMP to investigate the distribution of pH, porosity change, and free CO_2 over 1000-years following 10-year CO_2 injection. Results demonstrate the acidifying effect of CO_2 injection and its implications for the caprock–reservoir interface over time. The findings offer valuable perspectives on the feasibility and consequences of CO_2 geological storage in the Syderiai deep saline aquifer, highlighting the importance of incorporating leakage, geo-mechanical aspects, and geo-chemical aspects for implementing efficient CO_2 storage.

Keywords: CO_2 storage; Syderiai saline aquifer; leakage modeling; geo-mechanical modeling; geo-chemical modeling

Academic Editors: Nikolaos Koukouzas and Luca Fiori

Received: 19 October 2025
Revised: 27 November 2025
Accepted: 18 December 2025
Published: 23 December 2025

1. Introduction

In recent decades, fossil resources have played a predominant role in global energy consumption, accounting for a substantial 82% of the world's primary energy use in 2022 [1]. The combustion of fossil fuels has led to the significant release of carbon dioxide (CO_2) into the atmosphere, resulting in a notable increase in greenhouse gas concentrations and contributing to escalating temperatures and more frequent extreme weather events, presenting the world with an unprecedented environmental crisis. The atmospheric CO_2 concentrations were approximately 420.26 parts per million (ppm) in August 2024, rising to 422.95 ppm in August 2025, marking an increase of about 2.69 ppm in one year. This reflects

a 51.05% increase since the beginning of the Industrial Age, when the concentrations were approximately 280 ppm, and a 14.31% increase since 2000, when they were approximately 370 ppm [2]. Reducing CO_2 emissions by 2050, which is important to achieve the net zero target and reduce its impact on climate change, requires an annual reduction of ~1.4 Gt CO_2—equivalent to the emission decline observed in 2020 during COVID-19 lockdowns [3].

Carbon Capture and Storage (CCS) has emerged as one of the most promising methods in gaining momentum to reduce the concentration of CO_2 [4]. In CCS, CO_2 is captured and stored in the subsurface reservoirs such as the depleted hydrocarbon reservoir or the saline aquifer, being the most preferred locations for storing CO_2. To effectively store CO_2 in any reservoir, specific conditions must be met to ensure its suitability and long-term stability [5,6], such as a depth of 800 m or above, sealed by a caprock of very low permeability, and accessibility of the reservoir.

When storing CO_2 in subsurface reservoirs, leakage is a critical factor affecting stability and long-term efficiency [7,8]. Leakage can result from geo-mechanical impacts, such as fault reactivation and fracture propagation [9], or geo-chemical interactions that create escape pathways. The IPCC (2005) [10] recommends limiting CO_2 leakage to less than 1% over 1000 years, while the U.S. Department of Energy (US DOE) targets 99% retention. The European Union's CCS Directive [11] mandates permanent storage, making continuous monitoring essential to track leakage and ensure system integrity.

Leakage can pose environmental and health risks, such as groundwater contamination [12]. Pore pressure buildup during injection can lead to stress changes, increasing the risk of fault reactivation and shear failure at the caprock–reservoir interface [13], resulting in leakage of CO_2. Various studies have explored geo-mechanical effects, including work by [14–18]. A detailed review is provided by [19].

Moreover, geo-chemical interactions can also create leakage pathways [13]. The corrosive nature of CO_2 makes it essential to study its long-term impact on reservoir rocks [20,21]; it was found that albite's transformation into dawsonite reduced porosity, while Tremosa et al. [22] observed dawsonite precipitation in feldspar-rich sandstones but not in quartz-rich formations. This underscores the need for integrated geo-mechanical−geo-chemical risk analysis [23].

Analytical studies have focused on CO_2 release along wellbores [24–26], while theoretical models examine brine diffusion from aquifers into surrounding formations [27–29] and analyze pore pressure behavior before and after CO_2 injection, finding no significant impact on caprock integrity. Similarly, Vidal-Gilbert et al. [30] developed a 3D mechanical model and concluded that increased pore pressure does not compromise reservoir stability under ideal conditions. However, Rinaldi et al. [31] found that horizontal wells lead to larger seismic events and more widespread leakage through activated faults. Sun et al. [32] included subsurface uncertainty in geo-mechanical analysis and found that while caprock integrity remained stable, fault reactivation could still cause leakage. On comparing saline aquifers and depleted reservoirs, Orlic [33] observed higher pressure buildup in saline aquifers, which can exceed hydrostatic formation pressure and cause stress perturbations. Hangx et al. [34] found that calcite dissolution did not weaken rock strength, as quartz cementation preserved mechanical integrity. Although numerical simulations have explored CO_2 leakage through activated faults [31,35–37], significant challenges remain in characterizing leakage risks. Addressing these uncertainties is essential for ensuring the long-term security of CO_2 storage.

Despite extensive research on CO_2 storage, a comprehensive approach that integrates random fracture networks, geo-mechanical behavior, and geo-chemical reactions within the same study is lacking. The unpredictability of fracture networks, the influence of different grain packings, and the role of CO_2–brine–rock interactions remain underexplored. This

study fills these gaps by presenting a multi-faceted analysis of CO_2 sequestration risks, which is crucial for ensuring long-term storage security. This study is divided into three broad sections: CO_2 leakage assessment with complex random fracture network, geo-mechanical impact of CO_2 injection and storage, and geo-chemical alterations due to CO_2–brine–rock interactions.

The paper has been organized as follows: Section 1 introduces the problem statement and reviews the work performed in this study. Section 2 defines the area under study. The methodology adopted is described in Section 3, describing the leakage model, geo-mechanical model, and geo-chemical model. Section 4 discusses the results for different cases of leakage studies, geo-mechanical studies, and geo-chemical studies. Finally, the summary and conclusion are presented in Section 5.

2. Area Under Study

Lithuania comprises two onshore saline aquifers, Syderiai and Vaskai, which are considered potential sites for CO_2 geological storage in Lithuania [38–42]. Amongst the two onshore saline aquifers in Lithuania, the Syderiai saline aquifer offers maximum potential for storing CO_2. A study conducted by Malik et al. [41] using 3D mechanistic modeling indicated that with 30 years of CO_2 injection, the estimated CO_2 storage capacity of the Syderiai field ranges from 54 to 232 Mt. The broad range of storage capacity indicates the minimum and maximum values based on the uncertainty ranges for the reservoir properties. The literature [41,43] provides a detailed study of the CO_2 storage capacity of the Syderiai saline aquifer, making it the most suitable onshore saline aquifer for storing CO_2 based on the storage capacity estimates and its properties mentioned in Table 1.

Table 1. Properties of the Syderiai deep saline aquifer.

Structure	Syderiai Deep Saline Aquifer
Formation	Deimena
Stratigraphic Unit	Middle Cambrian
Lithology	Sandstone
Total Area	26 Square Kilometers
Top Depth	1458 m
Thickness	57 m
Porosity	0.16 Fraction
Permeability	400 mD
Net-to-Gross Ratio (NTG)	0.75
Temperature	50 °C
Pressure	150 bars
Salinity	122 g/L

The Syderiai deep saline aquifer is a subsurface layer containing brackish or saline water. It is a sandstone aquifer that is 1458 m deep. It is covered by a 560 m-thick layer of shaly rocks from the Ordovician to Silurian periods, which serves as a seal for potential CO_2 storage (Figure 1). Several larger-scale aquifers exist above this sealing package, but they are unsuitable for water supply due to high salinity. Drinking water is sourced from younger aquifers above the Upper Permian carbonaceous aquifer, which lies at depths of less than 90 m [43].

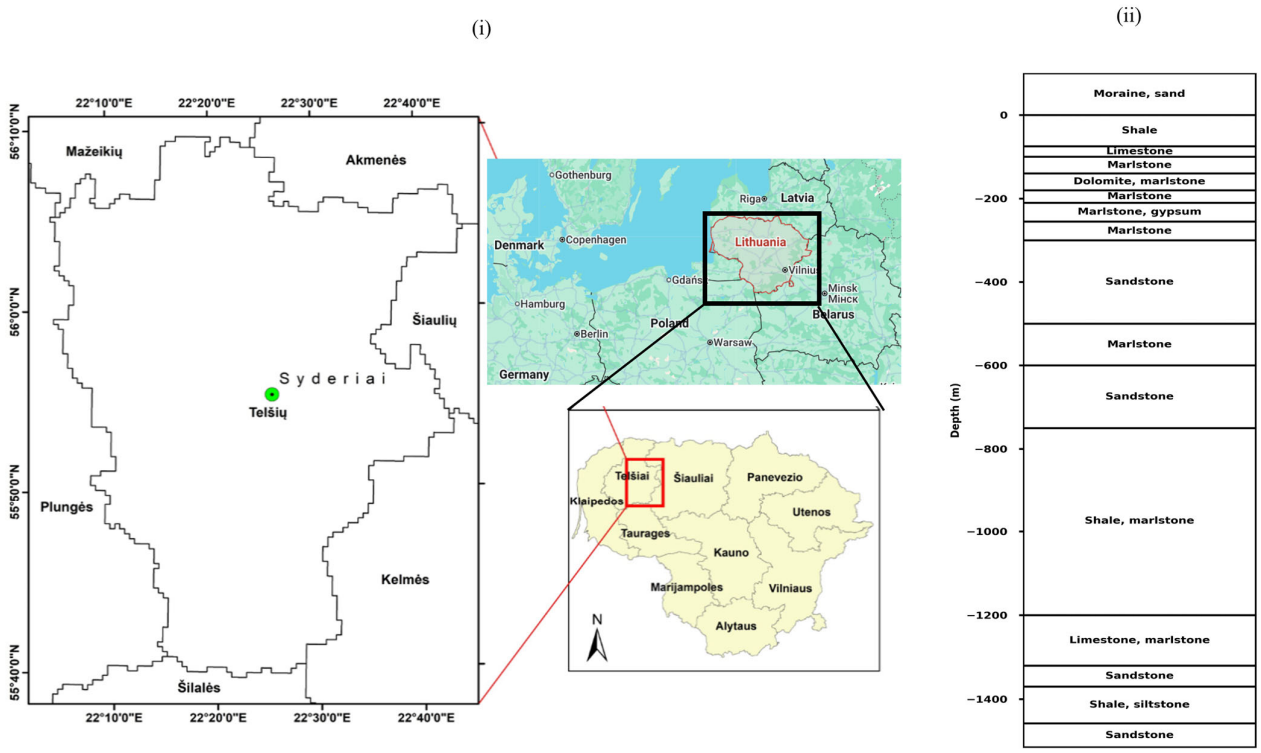

Figure 1. (**i**) Geographical location of the Syderiai field and (**ii**) the Lithology of Syderiai deep saline aquifer.

3. Methodology

In this study, three important aspects of long-term CO_2 storage integrity are analyzed, i.e., impact of leakage, geo-mechanical behavior, and geo-chemical behavior of CO_2 storage in the Syderiai saline aquifer of Lithuania. For leakage and geo-mechanical studies, a series of 3D mechanistic models were developed using the commercial simulation software T-navigator, whereas a 2D radial model was considered for analyzing the geo-chemical aspect of CO_2 storage using TOUGHREACT [44].

T-navigator [45] allows for the creation of detailed and comprehensive 3D models of the deep saline aquifer. The software provides tools and functionalities to incorporate various geological and reservoir data, such as porosity, permeability, and fluid properties, into the models. These models were specifically built to simulate and analyze the behavior of deep saline aquifers, focusing on their potential for CO_2 storage. The study employs T-navigator version 23.3 for leakage and geo-mechanical studies. All calculations were conducted using Python (version 3.x) and standard scientific libraries available in 2023, while the visualization of results was achieved through the utilization of the matplotlib and seaborn libraries for the geo-mechanical output and Tecplot [46] software (Tecplot 360 EX 2023 R2) for the geo-chemical output. A detailed description of the methodology adopted for each study is described in the following sub-sections.

3.1. Leakage Model Description

In this study, CO_2 was injected into the aquifer with the help of five injection wells drilled in a quarter-five-spot pattern and a complex fracture network was created (Figure 2). The Stochastic method was used for fracture network generation. This approach involves defining statistical distributions for key fracture properties such as orientation, length, spacing, and aperture. Using these distributions, a fracture network was generated using Python. Each fracture was defined by two points, and a constant fracture permeability value was assigned. This generated a fracture with the specified constant permeability

between the two points. This process was repeated to generate the complete fracture network [47,48].

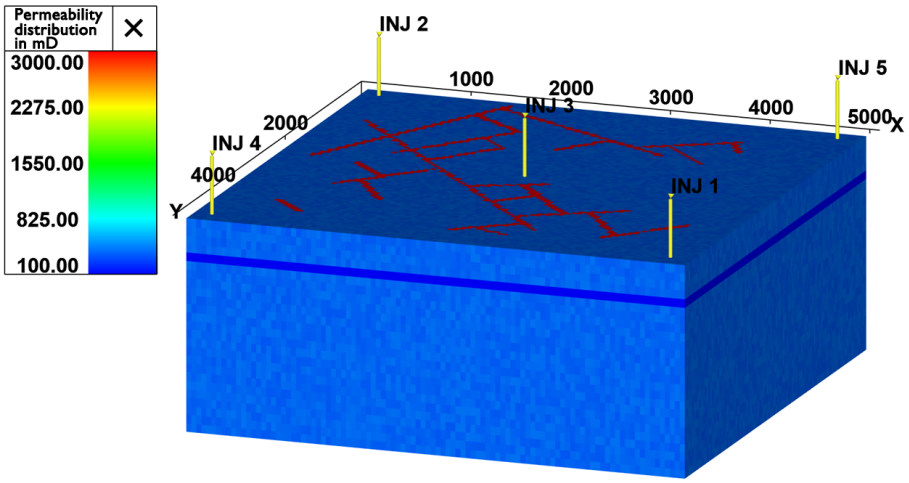

Figure 2. A 3D mechanistic model for the Syderiai deep saline aquifer showing the complex fracture network in red and the caprock layer in blue.

The injection process was regulated by the bottom hole pressure (BHP), which sets a limit on the maximum pressure allowed for CO_2 injection. The keyword "WCONINJE" was used to denote an injection well, and the specific well labeled such as "INJ 1" represented injection well 1 and so on. The injection well, "INJ 1," has a gas open rate profile described as "6500 1* 250". This profile indicates that the well is programmed to inject gas at a surface rate of 6500 Standard Cubic Meters per day (Sm^3/day) as long as the bottom hole pressure remains below 250 bars. These injection rates were based on data from the CO_2 injection trial conducted in the field, see [41,49,50]. However, if the bottom hole pressure exceeds the limit of 250 bars, the injection rate will be reduced to ensure compliance with the pressure constraint. The properties and operating parameters of the leakage model are described in Table 2.

Table 2. Properties and operating parameters of the leakage model.

Parameters		Value
Grid Dimensions	Nx	100
	Ny	100
	Nz	25
Number of cells		250,000
Formation Heterogeneity		10%
Perforation layers		4 (from layer 21–25)
Bottom hole pressure		250 bars
Injection period		15 years
Monitoring period		100 years

Moreover, in this study, the formation reservoir has an initial pressure of 153 bars (see [41,49,50]). To ensure adequate pressure for uninterrupted CO_2 injection over 15 years, a pressure margin of 100 bar was assumed. The bottom hole pressure (BHP) was adjusted to 250 bars. The selection of these pressure limits considers both reservoir injectivity and geo-mechanical stability and is based on field data; see reference [41,49,50]. Also, the injector wells were perforated in the bottom layers, specifically from layer

number 21 to layer number 25 (Figure 3). By targeting the bottom layers, the injection was focused on the lower portion of the aquifer, which can help optimize the distribution and containment of the injected CO_2. Other reservoir properties used in this model are mentioned in Table 1.

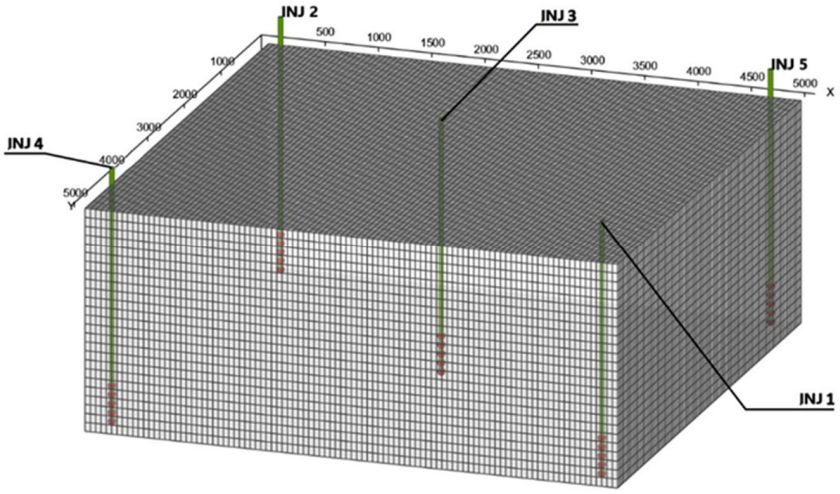

Figure 3. A 3D mechanistic model for the Syderiai deep saline aquifer; injection wells are shown in black color and perforation zone is shown in red color.

3.2. Geo-Mechanical Model Description

For the geo-mechanical study, the field measured values of permeability and porosity of the Syderiai field were used, as defined in Table 1. Additionally, the model generated for the leakage study was used to understand the impact of CO_2 injection on the mechanical properties of the reservoir. The grid dimensions are Nx = 100, Ny = 100, and Nz = 25 layers. This results in a total of 250,000 cells (100 × 100 × 25). In the study, the injector wells were perforated in the bottom layers, specifically from layer number 21 to layer number 25 (Figure 4). By targeting the bottom layers, the injection is focused on the lower portion of the aquifer, which can help optimize the distribution and containment of the injected CO_2.

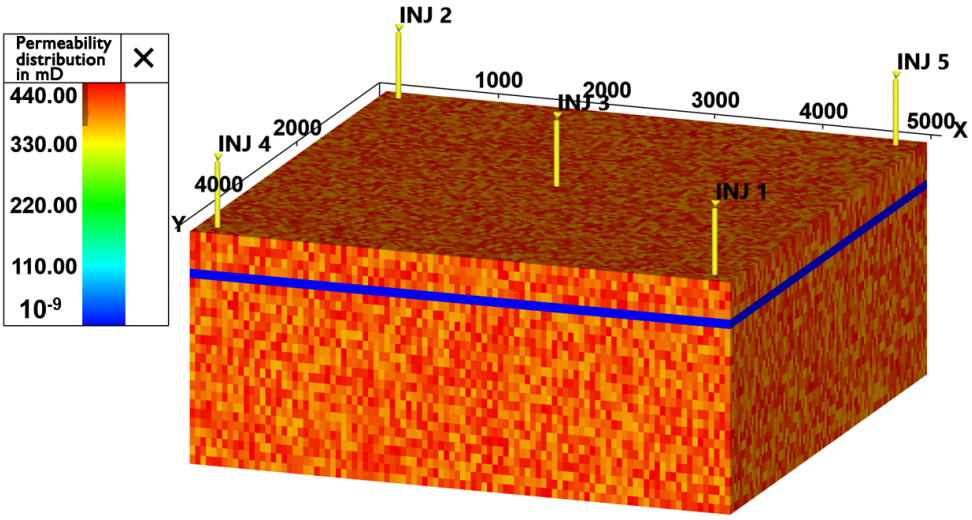

Figure 4. Heterogeneous permeability distribution along the *X*-axis for five-spot pattern in the bottom sandstone reservoir formation, shale caprock (blue), and the sandstone reservoir formation at the top above the caprock.

The temperature (T) of the field was calculated using Equation (1), where the geothermal gradient for equation was calculated from the geothermal gradient map of Lithuania [51].

$$T = G.(H - h_1) + t_0 \quad (1)$$

where H—depth; h_1—depth to "neutral" layer or to steady-state temperature zone, 30 m average; G—geothermal gradient, °C/km; t_0—mean annual surface temperature, +7.5 °C.

Sandstone rock compressibility was calculated using Equation (2) provided by [52];

$$C_f = \frac{97.32 \times 10^{-6}}{1 + 55.8721 \times \phi^{1.428586}}, Psi^{-1} \quad (2)$$

Equation (2) is valid for a porosity range of 2–23%, which is suitable for our formation.

Additionally, the coordination number (C) serves as a measure of the connectivity between pore bodies. In geological media with high permeability, like sand, individual pores are often connected to multiple surrounding pores, resulting in a higher coordination number (C > 6). This high coordination number indicates a more interconnected and permeable structure. Conversely, in geological media with low permeability, such as shale, the pore coordination number tends to be relatively small (C < 4). In low-permeability formations, individual pores are less likely to be connected to numerous neighboring pores, leading to a lower coordination number. This characteristic reflects the lower degree of connectivity and reduced fluid flow capability within the rock [53].

For salinity, NaCl and $CaCl_2$ concentrations in water were considered, and defined as 0.03 fraction and 0.02 fraction at 500 m, respectively, and 0.035 fraction and 0.025 fraction at 5000 m, respectively. Group injection was performed at a rate of 20,000 Sm^3/day. The injection shuts down when the bottom hole pressure reaches 250 bar. The model parameters and operating parameters are defined in Table 2 and the rock properties used for modeling are defined in Table 3.

Table 3. Rock properties for geo-mechanical study.

Rock Type	Sandstone	Shale
Rock density, kg/m^3	2650	2710
Young modulus (E), bar	500,000	100,000
Poisson ratio (v)	0.2	0.4
Coordination number (C)	6	4

3.3. Geo-Chemical Model Description

The 2D radial model depicting a cylindrical sandstone formation with a thickness of 57 m was assumed, schematics of the model are shown in Figure 5. The decision to use a radial 2D domain rather than a full 3D model was motivated by computational considerations: a fully coupled 3D reactive transport simulation for this system would require very large grid dimensions and extremely long computational run times due to the complexity of geo-chemical interactions. The radial 2D approach provides a computationally efficient alternative while still capturing the essential geo-chemical processes, including mineralogical alterations and porosity evolution induced by CO_2 injection. For the numerical simulation, the formation was discretized into 30 vertical layers, each with a consistent spacing of 2.28 m. The first five layers corresponded to shale caprock formation, followed by 25 layers representing sandstone formation. Horizontally, a radial distance of 73 km was simulated, with radial spacing increasing gradually away from the injection well. A total of 45 radial grid elements were employed, with the outermost grid element

set to a substantial volume of 1051 m^3, effectively representing an infinite lateral boundary to maintain constant pressure, temperature, and concentrations. The properties used in the modeling are given in Tables 4–6.

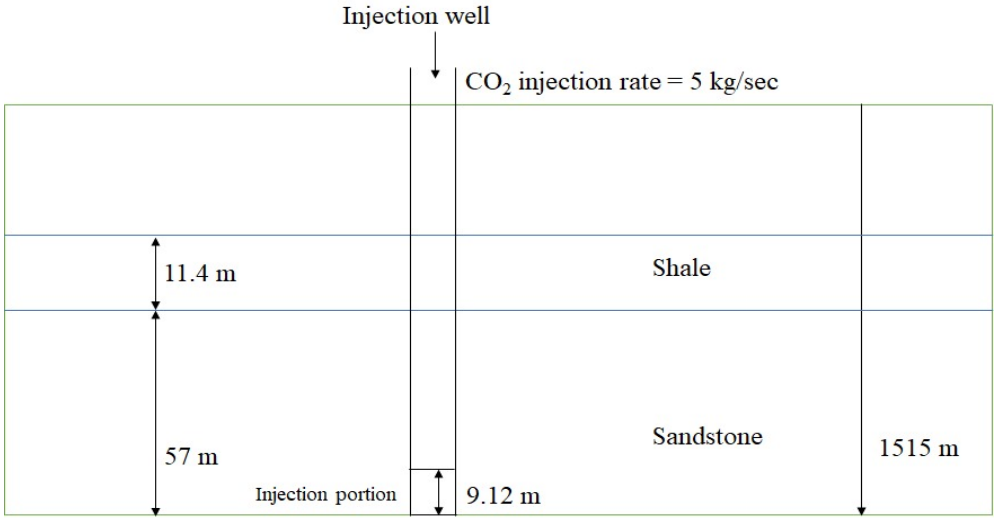

Figure 5. Schematic representation of the CO_2 injection simulation model.

Table 4. Rock properties.

Rock Type	Sandstone	Shale
Porosity, fraction	0.16	0.05
Permeability, mD	400	0.001
Rock density, kg/m^3	2650	2710
Compressibility, Pa^{-1}	2.78×10^{-9}	0.0×10^{-10}
Thickness, m	57	11.4

Table 5. Water composition.

	Units: mol/m^3							
pH	Cl^-	SO_4^{2-}	HCO_3^-	Na^+	K^+	Ca^{2+}	Mg^{2+}	Fe^{2+}
5.75	76,452	67.00	64.00	29,027	383	12,726.00	3128	3.00

Table 6. Initial conditions and injection specification.

Properties	Values
Pressure at well	153×10^5 Pa
Temperature	50 °C
Salinity	12.2 wt. % NaCl
CO_2 injection rate	5 Kg/s from each perforation layer
Number of perforation layers	4
Injection time	10 years

Minerals' composition was obtained through X-ray diffraction (XRD) on powdered rock samples of the formation. Table 7 shows XRD results on sandstone reservoir and shale caprock formation of the Syderiai Field.

Table 7. Mineral composition (wt%) of Sandstone Reservoir and Shale Caprock from XRD analysis.

Mineral	Sandstone Reservoir (wt%)	Shale Caprock (wt%)
Quartz	93.8	22.8
Kaolinite	1.1	–
Illite	1.8	77.2
Albite	3.2	–
Sepiolite	–	0.0

4. Results and Discussions

This study presents a comprehensive analysis addressing a critical aspect of CO_2 storage strategies. It builds upon prior research by [41], focusing on the estimation of storage capacities within Lithuanian reservoirs. This research extends its focus to scrutinize the potential risks entailed in the storage of CO_2. By examining various facets, our research aims to offer an understanding of the challenges and complexities associated with CCS initiatives. The results are divided into three sections, each addressing specific aspects of the storage process: leakage study, geo-mechanical study, and geo-chemical study.

4.1. Leakage Study

This section examines the behavior of CO_2 migration and potential leakage in a fractured reservoir system. Specifically, we analyzed how fracture permeability affects free CO_2 leakage volume, dissolved CO_2 leakage volume, and total CO_2 leakage. Simulations were conducted for a period of 115 years (2022–2136), consisting of 15 years of injection, followed by 100 years of post-injection monitoring.

4.1.1. Effect of Fracture Permeability on Free CO_2 Leakage Volume

This part evaluates how variations in fracture permeability influence the free CO_2 leakage volume, i.e., the volume of CO_2 that remains undissolved and migrates in its mobile phase. Figure 6 shows that increasing fracture permeability from 1000 mD to 20,000 mD causes a slight decrease in free CO_2 leakage volume. High-permeability fractures promote more efficient CO_2 migration within the reservoir, enhancing trapping and dissolution within the porous matrix. In contrast, low-permeability formations restrict fluid flow, increase capillary forces, and promote CO_2 accumulation near the injection zone, thereby enhancing buoyancy-driven leakage. Although the trend indicates reduced leakage with higher permeability, the change is on the order of 10^{-4}, suggesting that the permeability effect is negligible. At 1000 mD, the fracture already behaves as a dominant leakage pathway; thus, further increase in permeability do not significantly alter the free CO_2 leakage volume. Beyond 1000 mD, the leakage behavior is no longer governed by fracture permeability but by other controlling mechanisms such as buoyancy-driven flow, capillary pressure at the fracture–matrix boundary, and the rate of CO_2 dissolution into the surrounding porous matrix.

4.1.2. Effect of Fracture Permeability on Dissolved CO_2 Leakage Volume

In this section, we present the results of our investigation into the dissolved CO_2 leakage volume within varying fracture permeabilities over a period of 115 years. The study encompasses a range of fracture permeabilities spanning from 1000 mD to 20,000 mD. Figure 7 shows that as the fracture permeability increases, the dissolved CO_2 leakage volume also increases. This increasing trend suggests that there is high CO_2–brine interaction at high permeability, leading to greater CO_2 dissolution. However, the increase is limited to the order of 10^{-2}, indicating that dissolution is constrained by mass-transfer limitations

and CO_2 solubility limits. Consequently, despite higher permeability, only a marginal increase in dissolved CO_2 leakage is observed.

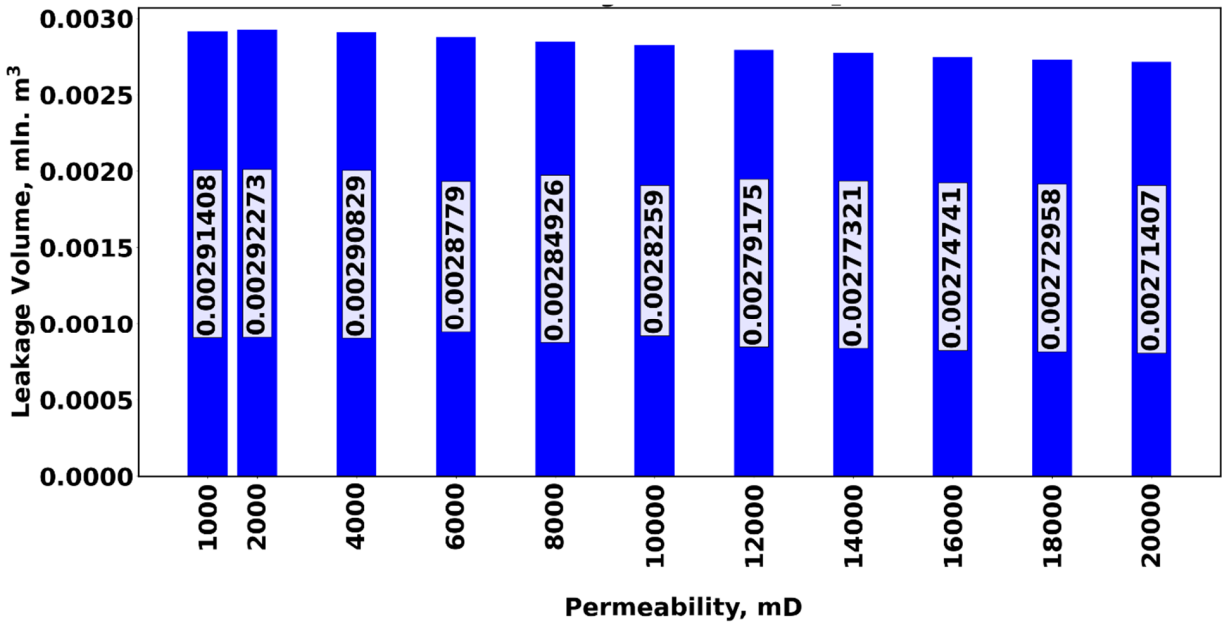

Figure 6. Free CO_2 leakage volume (mln. m^3) for different fracture permeabilities.

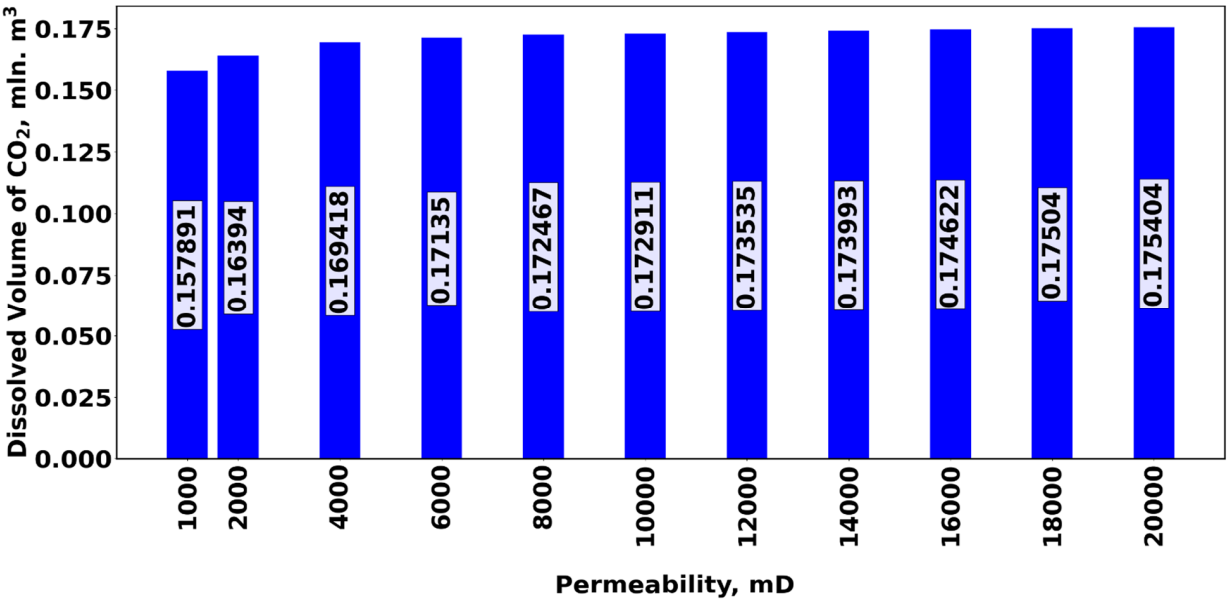

Figure 7. Dissolved CO_2 leakage volume (mln. m^3) for different fracture permeabilities.

4.1.3. Total CO_2 Leakage Volume

The total CO_2 leakage volume consists of both the free and dissolved CO_2 components. Figure 8 provides a comprehensive overview of these results. It is observed that the total leakage volume increases slightly with fracture permeability, primarily due to dominant dissolved CO_2 leakage. However, the total change remains on the order of 10^{-2}–10^{-3}, indicating that once the fracture is sufficiently permeable, further increase in permeability has little effect on the total leakage volume.

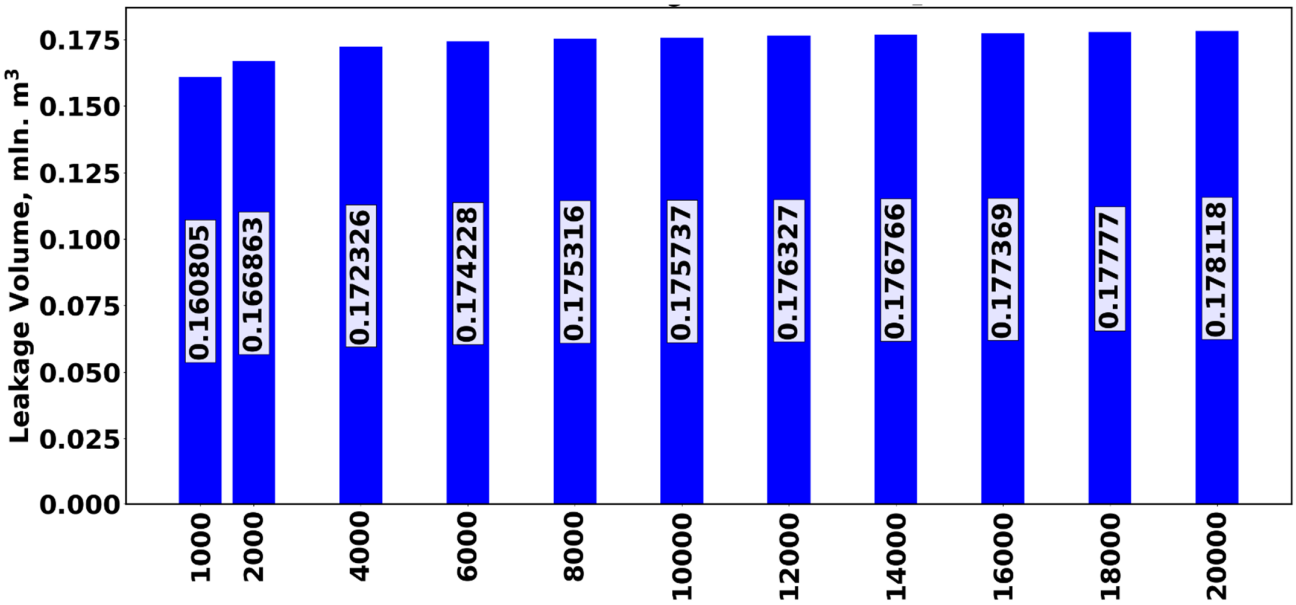

Figure 8. Total leakage volume of CO_2 for different fracture permeability.

4.2. Geo-Mechanical Study

This section investigates how CO_2 injections affect the mechanical behavior of formations composed of loose and packed grains. The bulk modulus and shear modulus of the rock are key indicators of its mechanical strength and deformation response. Therefore, we monitored how these properties evolve after CO_2 injection for different grain-packing conditions in shale (caprock) and sandstone (reservoir). The simulation covered 115 years, from 2022 to 2136, including a 15-year injection period, followed by 100 years of monitoring.

Loose grains here refer to unconsolidated grains with low porosity that lack strong interparticle bonding (grain–grain contact area). They typically occur when sediments accumulate without undergoing the compaction and cementation processes necessary for solid rock formation, thus reducing their stiffness. In contrast, packed grains have undergone compaction and cementation, resulting in solid rock formation with high stiffness. Compaction occurs as sediments accumulate and are compressed by overlying material, while cementation involves mineral precipitation (e.g., silica, calcium carbonate, or iron oxide), binding sand grains together [54].

CO_2 injection into the formation increases pore pressure in the sandstone, thereby reducing the effective pressure, as evident in our results. Notably, significant differences were observed in modulus changes between packed and loose sandstone grains following CO_2 injection. The increase in bulk modulus in packed sandstone (Figure 9) indicates initial consolidation or cementation, which reduces pore space and strengthens the rock. Conversely, the decrease in shear modulus in packed sandstone suggests a reduced ability to resist shape deformation, possibly due to cementation or clay transformations that lower shear strength. In loose sandstone, both bulk and shear modulus decrease over time, indicating a lack of compaction (Figure 9).

In the shale formation, which serves as the caprock, an increase in effective pressure leads to an increase in both bulk modulus and shear modulus for packed shale (Figure 10). This behavior indicates progressive stiffening over time, likely caused by consolidation and compaction. In contrast, a slight decrease in both bulk modulus and shear modulus is observed in loose shale over the 115-year period, suggesting that loose grains experience minimal compaction during long-term CO_2 exposure.

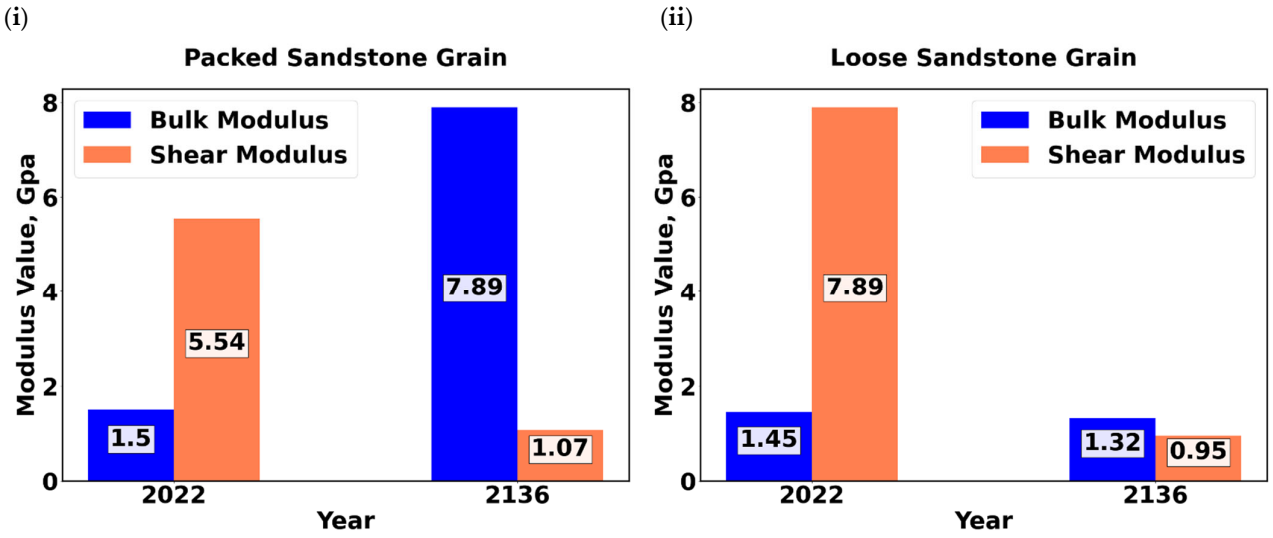

Figure 9. Bulk modulus and shear modulus change in 115 years for (**i**) packed sandstone grain and (**ii**) loose Sandstone grain.

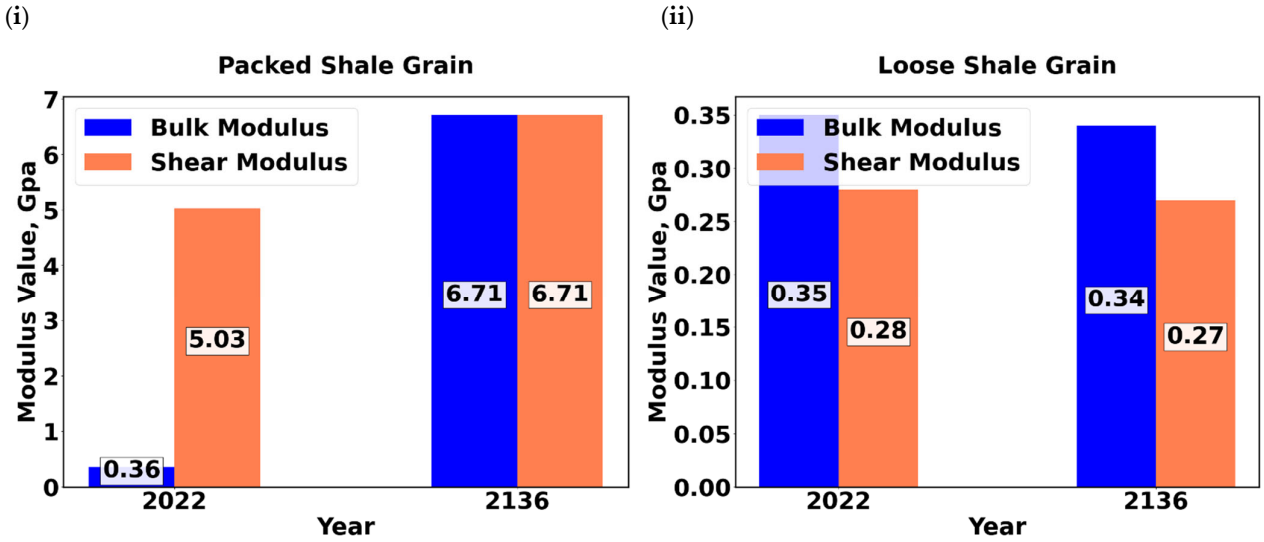

Figure 10. Bulk modulus and shear modulus change in 115 years for (**i**) packed Shale grain and (**ii**) loose shale grain.

4.3. Geo-Chemical Study

The geo-chemical impact was studied using a 2D radial model; while a 2D model cannot capture the spatial heterogeneity of long-term fluid migration, it adequately represents the dominant geo-chemical processes governing mineral trapping and caprock–reservoir interactions near the injection zone.

CO_2 injections occurred at the bottom section, spanning a thickness of 9.12 m, at a steady rate of 5 kg/s in each perforation layer (equivalent to a total of 0.63 Mt/year) over 10 years (Figure 5). The simulation spanned 1000 years, aligning with the typical time scale of interest for CO_2 geological sequestration studies. Initially, a homogeneous field was assumed, with subsequent heterogeneity arising from changes in porosity and permeability due to mineral alteration, promoting convective mixing. A constant temperature of 50 °C was applied across the entire domain and throughout the simulation, approximating reservoir depth conditions.

The distribution of various properties, such as pH, porosity change, free CO_2, and quartz concentration was observed over a span of 1000 years, as depicted in Figures 11–14.

The CO_2 injection was performed for 10 years, followed by a 990-year monitoring period. From Figures 11–14, it is observed that variations in these parameters primarily occurred at the injection point, with properties remaining relatively constant as distance from the wellbore increased.

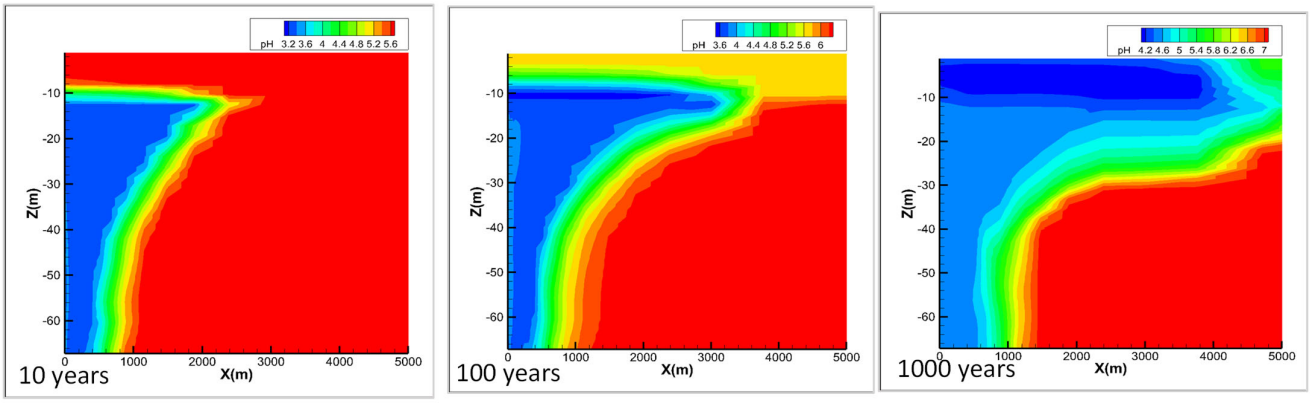

Figure 11. Distribution of pH at 10, 100 and 1000 years for the 2D injection model.

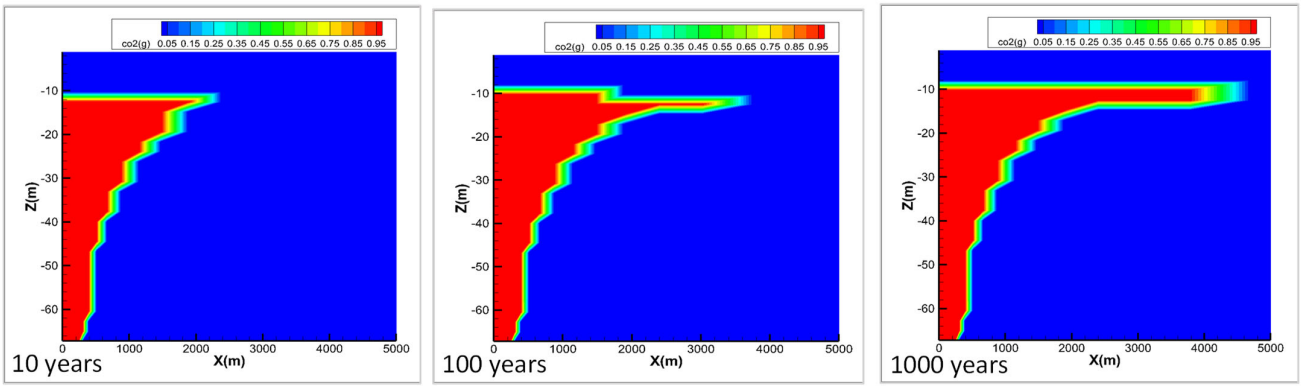

Figure 12. Distribution of free CO_2 at 10, 100 and 1000 years for the 2D injection model.

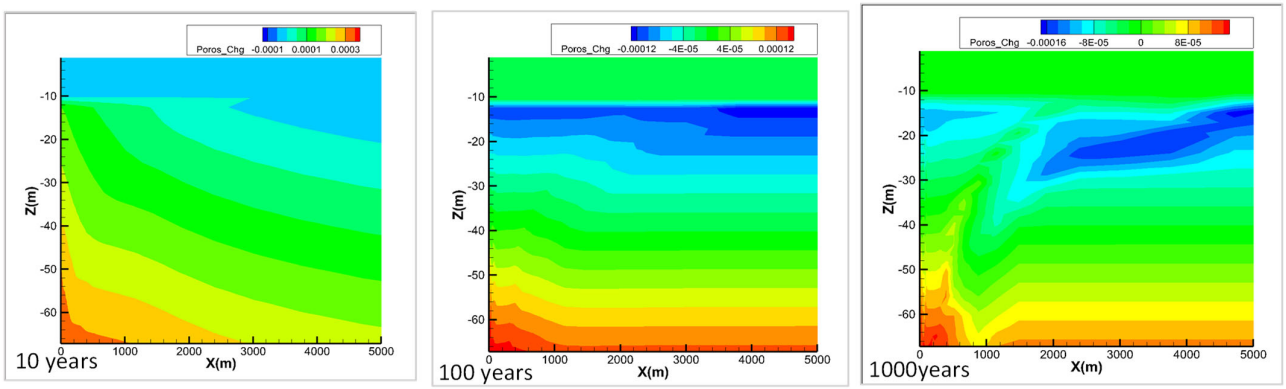

Figure 13. Distribution of porosity change at 10, 100 and 1000 years for the 2D injection model.

The introduction of CO_2 at the injection site led to a decrease in pH within the formation after 10 years of CO_2 injection, whereas farther from the wellbore, the formation's pH remained nearly neutral. This illustrates the acidifying effect of CO_2 injections (Figure 11). After 10 years of continuous injection, the monitoring phase begins, during which a change in pH gradually spreads as CO_2 migrates. CO_2 tends to move upwards due to the buoyancy effect, resulting in increased acidity at the caprock–reservoir interface. Figure 12 shows the behavior of free CO_2 over the 1000-year timeframe. The CO_2 initially gets accumulated near the injection site, and after injection phase, it migrates. Buoyancy causes it to

ascend (Figure 12), and it gets accumulated near the interface of the formation and caprock. Figure 13 shows the changes in porosity observed over the 1000-year period. It is observed that the porosity change is of the order of 10^{-3} to 10^{-5}, with maximum change occurring near the injection site after 10 years of continuous injection. This change could be due to possible dissolution of minerals due to acidification of formation near the injection site. During the observation phase, as CO_2 begins to migrate, the change in porosity gradually decreases (Figure 13). These changes are small and do not substantially affect the flow properties. Moreover, Figure 14 shows the effect of CO_2 injection on the quartz concentration and observed a minimal precipitation of quartz near the injection site after 10 years of injection. The concentration further increases over the 990-year monitoring phase as CO_2 migrates and interacts with brine and rocks and results in the formation of quartz minerals as a by-product of clay mineral dissolution. This signifies progressive stabilization of the geo-chemical system as CO_2 migrates and reacts with formation minerals.

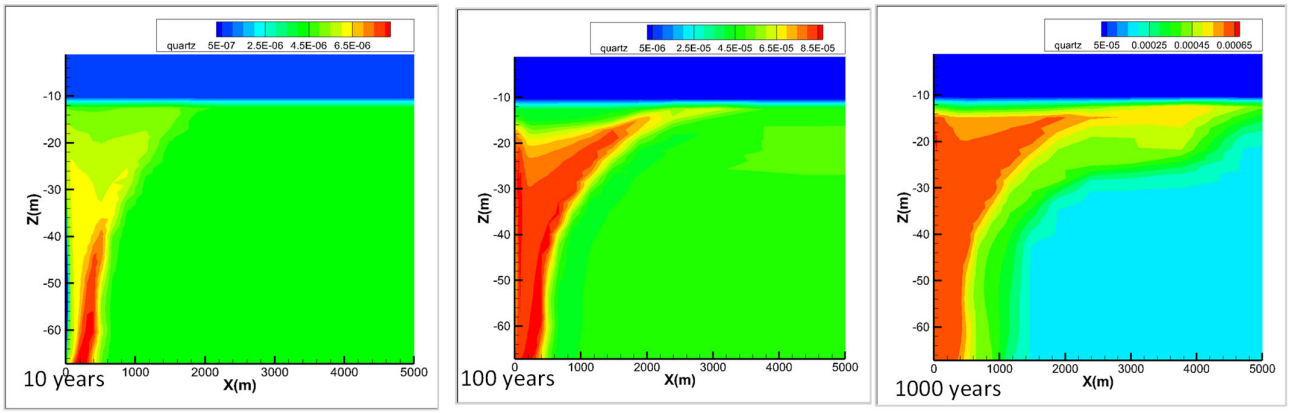

Figure 14. Distribution of quartz concentration at 10, 100 and 1000 years for the 2D radial model.

The trends suggest that the geo-chemical reactions are more localized around the injection zone, and the overall magnitude of the observed changes indicates that the long-term geo-chemical impact remains minimal, thus making the reservoir suitable for CO_2 storage.

5. Summary and Conclusions

The study provides a comprehensive analysis of the risks associated with the long-term storage of CO_2 into Lithuania's deep saline aquifer, Syderiai. Syderiai, an onshore saline aquifer, exhibits maximum potential for storing CO_2 compared to other reservoirs in Lithuania, as discussed in the literature. The study focuses on three important aspects of long-term CO_2 storage integrity, leakage, geo-mechanical and geo-chemical behavior. The leakage and geo-mechanical studies were performed for a total of 115 years, consisting of a 15-year injection period followed by a 100-year monitoring period, whereas for geo-chemical study, the simulation was performed for 1000 years, consisting of a 10-year injection period and a 990-year monitoring phase. The following conclusions can be drawn from the present research work:

1. The total CO_2 leakage volume (i.e., the combined free-phase and dissolved-phase CO_2) increases with fracture permeability primarily due to the dominance of dissolved CO_2 transport, even though the overall change remains small.
2. Shale grains see more strengthening over time compared to sandstone, likely due to clay mineral transformations that help bind the structure. Additionally, sandstone shows extreme shear modulus reduction in packed grains, possibly due to quartz overgrowths locking grains together without improving shear strength.

3. The geo-chemical study shows that maximum changes in properties such as pH, free- CO_2 concentration, porosity change and quartz concentration are observed near the injection site whereas the properties remaining relatively constant farther into the formation. During the monitoring phase, the injected CO_2 migrates and travels farther into the formation or due to buoyancy effect gets accumulated near the caprock–reservoir interface, thus causing minimal changes in the properties at these locations.

Although the leakage and geo-mechanical models were developed in three-dimension and the geo-chemical model employed a 2D radial configuration, this approach was selected to balance computational efficiency with the need to capture essential reactive transport processes. Future work could extend the present study by developing fully coupled 3D geo-mechanical–geo-chemical simulations, enabling a more integrated evaluation of injection performance and long-term CO_2 storage integrity.

The findings of this study contribute valuable insights into the feasibility and implications of CO_2 geological storage in the Syderiai deep saline aquifer, emphasizing the importance of considering leakage, geo-mechanical, and geo-chemical factors for effective CO_2 storage and risk management strategies.

Author Contributions: Conceptualization, S.L.D., M.P., S.M. and R.S.; methodology, S.L.D. and R.S.; software, S.L.D.; validation, S.L.D. and M.P.; formal analysis, S.L.D.; investigation, S.L.D. and S.M.; resources, R.S.; data curation, S.L.D.; writing—original draft preparation, S.M., M.P., R.S. and S.L.D.; writing—review and editing, S.L.D. and S.M.; visualization, S.L.D.; supervision, M.P. and R.S.; project administration, M.P.; funding acquisition, M.P. All authors have read and agreed to the published version of the manuscript.

Funding: This research was funded by the Lithuanian Research Council. Grant no. P-PD-22-022.

Institutional Review Board Statement: Not applicable.

Informed Consent Statement: Not applicable.

Data Availability Statement: The data presented in this study are available on request from the corresponding author.

Acknowledgments: The authors would like to acknowledge the support from UAB Minijos Nafta for sharing data for reservoir modeling and simulation. Special thanks are extended to the Rock and Fluid Multiphysics Laboratory (RFML), IIT Roorkee for their assistance in providing access to essential facilities, laboratory experiments, and expertise, which significantly contributed to this research.

Conflicts of Interest: The authors declare no conflicts of interest.

References

1. BP. *BP Statistical Review of World Energy 2022*, 71st ed.; London, UK, 2022.
2. Lan, X.; Tans, P.; Thoning, K.W. *Trends in Globally-Averaged CO_2 Determined from NOAA Global Monitoring Laboratory Measurements*; Version Thursday, 13-Nov-2025 16:04:26 MST; NOAA Global Monitoring Laboratory: Boulder, CO, USA, 2025. [CrossRef]
3. Global Carbon Project. Global Carbon Budget. November 2022. Available online: https://globalcarbonbudget.org/carbonbudget/ (accessed on 10 July 2023).
4. Pal, M.; Karaliūtė, V.; Malik, S. Exploring the potential of carbon capture, utilization, and storage in Baltic Sea region countries: A review of CCUS patents from 2000 to 2022. *Processes* **2023**, *11*, 605. [CrossRef]
5. Chadwick, A.; Arts, R.; Bernstone, C.; May, F.; Thibeau, S.; Zweigel, P. *Best Practice for the CO_2 Storage in Saline Aquifers—Observations and Guidelines from the SACS and CO2STORE Projects*; British Geological Survey: Nottingham, UK, 2008.
6. IEA Greenhouse Gas R&D Programme (IEA GHG). *CCS Site Characterization Criteria*; IEA GHG: Cheltenham, UK, 2009.
7. Dangi, S.L.; Malik, S.; Makauskas, P.; Karliute, V.; Sharma, R.; Pal, M. Assessment of CO_2 leakage using mechanistic modelling approach for CO_2 injection in deep saline aquifer of Lithuanian basin in presence of fault and fractures. In Proceedings of the Baltic Carbon Forum, Riga, Latvia, 15–16 February 2023. [CrossRef]

8. Dangi, S.L.; Malik, S.; Makauskas, P.; Karliute, V.; Sharma, R.; Pal, M. An approach for assessment of CO_2 leakage using mechanistic modelling: CO_2 injection in deep saline aquifer of Lithuanian basin in presence of fault and fractures. *Adv. Carbon Capture Util. Storage* **2024**, *2*, 1–8. [CrossRef]
9. Shi, J.Q.; Durucan, S. A coupled reservoir-geomechanical simulation study of CO_2 storage in a nearly depleted natural gas reservoir. *Energy Procedia* **2009**, *1*, 3039–3046. [CrossRef]
10. Intergovernmental Panel on Climate Change (IPCC). *Carbon Dioxide Capture and Storage*; Cambridge University Press: Cambridge, UK, 2005.
11. European Union's CCS Directive. 2009. Available online: http://data.europa.eu/eli/dir/2009/31/oj (accessed on 5 March 2024).
12. Mortezaei, K.; Amirlatifi, A.; Ghazanfari, E.; Vahedifard, F. Potential CO_2 leakage from geological storage sites: Advances and challenges. *Environ. Geotech.* **2021**, *8*, 3–27. [CrossRef]
13. Song, Y.; Jun, S.; Na, Y.; Kim, K.; Jang, Y.; Wang, J. Geomechanical challenges during geological CO_2 storage: A review. *Chem. Eng. J.* **2023**, *456*, 140968. [CrossRef]
14. Rutqvist, J.; Tsang, C.F. A study of caprock hydromechanical changes associated with CO_2-injection into a brine formation. *Environ. Geol.* **2002**, *42*, 296–305. [CrossRef]
15. Hawkes, C.D.; McLellan, P.J.; Zimmer, U.; Bachu, S. Geomechanical factors affecting geological storage of CO_2 in depleted oil and gas reservoirs: Risks and mechanisms. In Proceedings of the ARMA North America Rock Mechanics Symposium, Houston, TX, USA, 14–16 October 2024; ARMA: Tampa, FL, USA, 2024; p. ARMA-04.
16. Hawkes, C.D.; McLellan, P.J.; Bachu, S. Geomechanical factors affecting geological storage of CO_2 in depleted oil and gas reservoirs. *J. Can. Pet. Technol.* **2005**, *44*, PETSOC-05-10-05. [CrossRef]
17. Rutqvist, J.; Birkholzer, J.T.; Tsang, C.F. Coupled reservoir–geomechanical analysis of the potential for tensile and shear failure associated with CO_2 injection in multilayered reservoir–caprock systems. *Int. J. Rock Mech. Min. Sci.* **2008**, *45*, 132–143. [CrossRef]
18. Sharma, R.; Dangi, S.L.; Nagarkoti, N.; Malik, S.; Pandey, P.; Pal, M. Caprock and Associate Geomechanical Risks in Carbon Capture and Sequestration (CCS) Implementation: A Study on Loose and Packed Sandstone Grain. In Proceedings of the American Geophysical Union Fall Meeting (AGU), San Francisco, CA, USA, 11–15 December 2023.
19. Dangi, S.L.; Malik, S.; Sharma, R.; Pal, M. Geomechanical Implications of CO_2 Sequestration in Saline Aquifers. In Proceedings of the 14th Biennial International Conference (SPG 2023), Kochi, India, 3–5 November 2023.
20. Gaus, I.; Audigane, P.; André, L.; Lions, J.; Jacquemet, N.; Durst, P.; Czernichowski-Lauriol, I.; Azaroual, M. Geochemical and solute transport modelling for CO_2 storage, what to expect from it? *Int. J. Greenh. Gas Control* **2008**, *2*, 605–625. [CrossRef]
21. Tambach, T.; Koenen, M.; Bergen, F.V. Geochemical evaluation of CO_2 injection into storage reservoirs based on case-studies in the Netherlands. *Energy Procedia* **2011**, *4*, 4747–4753. [CrossRef]
22. Tremosa, J.; Castillo, C.; Quang Vong, C.; Kervevan, C.; Lassin, A.; Audigane, P. Long-term Assessment of Geochemical Reactivity of CO_2 Storage in Highly Saline Aquifers: Application to Ketzin, In Salah and Snøhvit storage sites. *Int. J. Greenh. Gas Control* **2014**, *20*, 2–26. [CrossRef]
23. Gholami, R.; Raza, A.; Iglauer, S. Leakage risk assessment of a CO_2 storage site: A review. *Earth-Sci. Rev.* **2021**, *223*, 103849. [CrossRef]
24. Nordbotten, J.M.; Celia, M.A.; Bachu, S. Analytical solutions for leakage rates through abandoned wells. *Water Resour. Res.* **2004**, *40*. [CrossRef]
25. Nordbotten, J.M.; Celia, M.A.; Bachu, S.; Dahle, H.K. Semianalytical solution for CO_2 leakage through an abandoned well. *Environ. Sci. Technol.* **2005**, *39*, 602–611. [CrossRef]
26. Nordbotten, J.M.; Kavetski, D.; Celia, M.A.; Bachu, S. Model for CO_2 leakage including multiple geological layers and multiple leaky wells. *Environ. Sci. Technol.* **2009**, *43*, 743–749. [CrossRef]
27. Dejam, M.; Hassanzadeh, H. Diffusive leakage of brine from aquifers during CO_2 geological storage. *Adv. Water Resour.* **2018**, *111*, 36–57. [CrossRef]
28. Dejam, M.; Hassanzadeh, H. The role of natural fractures of finite double-porosity aquifers on diffusive leakage of brine during geological storage of CO_2. *Int. J. Greenh. Gas Control* **2018**, *78*, 177–197. [CrossRef]
29. Ganguli, S.S.; Sen, S.; Kumar, M. Geomechanical analysis for feasible CO_2 storage in an Indian mature oil field. In Proceedings of the 12th Biennial International Conference & Exposition (SPG), Jaipur, India, 17 November 2017; Volume 19.
30. Vidal-Gilbert, S.; Nauroy, J.F.; Brosse, E. 3D geomechanical modelling for CO_2 geologic storage in the Dogger carbonates of the Paris Basin. *Int. J. Greenh. Gas Control* **2009**, *3*, 288–299. [CrossRef]
31. Rinaldi, A.P.; Vilarrasa, V.; Rutqvist, J.; Cappa, F. Fault reactivation during CO_2 sequestration: Effects of well orientation on seismicity and leakage. *Greenh. Gases Sci. Technol.* **2015**, *5*, 645–656. [CrossRef]
32. Sun, Z.; Salazar-Tio, R.; Wu, L.; Bostrøm, B.; Fager, A.; Crouse, B. Geomechanical assessment of a large-scale CO_2 storage and insights from uncertainty analysis. *Geoenergy Sci. Eng.* **2023**, *224*, 211596. [CrossRef]
33. Orlic, B. Geomechanical effects of CO_2 storage in depleted gas reservoirs in the Netherlands: Inferences from feasibility studies and comparison with aquifer storage. *J. Rock Mech. Geotech. Eng.* **2016**, *8*, 846–859. [CrossRef]

34. Hangx, S.; Linden, A.V.D.; Marcelis, F.; Bauer, A. The effect of CO_2 on the mechanical properties of the Captain Sandstone: Geological storage of CO_2 at the Goldeneye field (UK). *Int. J. Greenh. Gas Control* **2013**, *19*, 609–619. [CrossRef]
35. Kang, M.; Nordbotten, J.M.; Doster, F.; Celia, M.A. Analytical solutions for two-phase subsurface flow to a leaky fault considering vertical flow effects and fault properties. *Water Resour. Res.* **2014**, *50*, 3536–3552. [CrossRef]
36. Rinaldi, A.P.; Jeanne, P.; Rutqvist, J.; Cappa, F.; Guglielmi, Y. Effects of fault-zone architecture on earthquake magnitude and gas leakage related to CO_2 injection in a multi-layered sedimentary system. *Greenh. Gases Sci. Technol.* **2014**, *4*, 99–120. [CrossRef]
37. Rutqvist, J.; Rinaldi, A.P.; Cappa, F.; Jeanne, P.; Mazzoldi, A.; Urpi, L.; Guglielmi, Y.; Vilarrasa, V. Fault activation and induced seismicity in geologic carbon storage—Lessons learned from recent modeling studies. *J. Rock Mech. Geotech. Eng.* **2016**, *8*, 789–804. [CrossRef]
38. Shogenova, A.; Šliaupa, S.; Shogenov, K.; Šliaupienė, R.; Pomeranceva, R.; Uibu, M.; Kuusik, R. Possibilities for geological storage and mineral trapping of industrial CO_2 emissions in the Baltic region. *Energy Procedia* **2009**, *1*, 2753–2760. [CrossRef]
39. Shogenova, A.; Sliaupa, S.; Vaher, R.; Shogenov, K.; Pomeranceva, R. The Baltic basin: Structure, properties of reservoir rocks, and capacity for geological storage of CO_2. *Est. J. Earth Sci.* **2009**, *58*, 259–267. [CrossRef]
40. Šliaupa, S.; Šliaupiene, R. Prospects of Geological Storage of CO_2 in Lithuania. In Proceedings of the Baltic Carbon Forum, Online, 15 October 2021.
41. Malik, S.; Makauskas, P.; Karaliūtė, V.; Pal, M.; Sharma, R. Assessing the Geological Storage Potential of CO_2 in Baltic Basin: A Case Study of Lithuanian Hydrocarbon and Deep Saline Reservoirs. *Int. J. Greenh. Gas Control* **2024**, *133*, 104097. [CrossRef]
42. Malik, S.; Makauskas, P.; Sharma, R.; Pal, M. Evaluating Petrophysical Properties Using Digital Rock Physics Analysis: A CO_2 Storage Feasibility Study of Lithuanian Reservoirs. *Appl. Sci.* **2024**, *14*, 10826. [CrossRef]
43. Šliaupienė, R.; Šliaupa, S. Prospects for CO_2 geological storage in deep saline aquifers of Lithuania and adjacent territories. *Geologija* **2011**, *53*, 121–133. [CrossRef]
44. TOUGHREACT V4.13-OMP, TOUGH 2024, Academic License provided by Lawrence Berkeley National Laboratory. Available online: https://tough.lbl.gov/software/toughreact_v4-13-omp/ (accessed on 2 March 2024).
45. T-navigator version 23.3. *Rock Flow Dynamics*; Rock Flow Dynamics, Inc.: Houston, TX, USA, 2023; Available online: https://rfdyn.com/ (accessed on 1 February 2024).
46. Tecplot. *Tecplot 360 EX R2*; Tecplot, Inc.: Bellevue, WA, USA, 2023.
47. Pal, M.; Jadhav, S. An efficient workflow for meshing large scale discrete fracture networks for solving subsurface flow problems. *Pet. Sci. Technol.* **2022**, *40*, 1945–1978. [CrossRef]
48. Ahmed, R.; Edwards, M.G.; Lamine, S.; Huisman, B.A.H.; Pal, M. Control-volume distributed multi-point flux approximation coupled with a lower-dimensional fracture model. *J. Comput. Phys.* **2015**, *284*, 462–489. [CrossRef]
49. Haselton, M.T. Exploiting the ROZ in Lithuanian. In Proceedings of the 19th Annual CO_2 Flooding Conference, Midland, TX, USA, 11–13 December 2013.
50. Ignas, V.; Rimas, G. Minijos Nafta and its experience in CO_2 injection. In Proceedings of the Baltic Carbon Forum, Vilnius, Lithuania, 3–4 October 2024.
51. Rasteniene, V.; Puronas, V. *Geothermal Atlas of Lithuania*; World Geothermal Congress: Antalya, Turkey, 2005; pp. 24–29.
52. Newman, G.H. Pore-volume compressibility of consolidated, friable, and unconsolidated reservoir rocks under hydrostatic loading. *J. Pet. Technol.* **1973**, *25*, 129–134. [CrossRef]
53. Tiab, D.; Donaldson, E.C. Effect of Stress on Reservoir Rock Properties. In *Petrophysics*; Gulf Professional Publishing: Oxford, UK, 2016; pp. 483–582. [CrossRef]
54. Mavko, G.; Mukerji, T.; Dvorkin, J. *The Rock Physics Handbook: Tools for Analysis in Porous Media*; Cambridge University Press: Cambridge, UK, 1988.